Heteroanionic Materials Based on Copper Clusters, Bisphosphonates, and Polyoxometalates: Magnetic Properties and Comparative Electrocatalytic NO x Reduction Studies

Olivier Oms, Shu Yang, William Salomon, Jérôme Marrot, Anne Dolbecq, Eric Rivière, Antoine Bonnefont, Laurent Ruhlmann, Pierre Mialane

Heteroanionic Materials Based on Copper Clusters, Bisphosphonates and Polyoxometalates: Magnetic Properties and Comparative Electrocatalytic Studies NOx Reduction Studies

Olivier Oms,[†,¶] Shu Yang,[§,¶] William Salomon,[†] Jérôme Marrot,[†] Anne Dolbecq,[†] Eric Rivière,[‡] Antoine Bonnefont,[§] Laurent Ruhlmann,*[§] and Pierre Mialane*[†]

[†] *Institut Lavoisier de Versailles, UMR 8180, Université de Versailles Saint-Quentin en Yvelines, Université Paris-Saclay, 45 Avenue des Etats-Unis, 78035 Versailles cedex, France. E-mail : pierre.mialane@uvsq.fr*

[‡] *Institut de Chimie Moléculaire et des Matériaux d'Orsay, UMR 8182, Equipe Chimie Inorganique, Univ. Paris-Sud, 91405 Orsay cedex, France.*

[§] *Université de Strasbourg, Institut de Chimie, UMR CNRS 7177, Laboratoire d'Electrochimie et de Chimie Physique du Corps Solide, 4 rue Blaise Pascal, CS 90032, 67081 Strasbourg cedex, France. E-mail :lruhlmann@unistra.fr*

[¶] *These authors contribute equally to this work.*

ABSTRACT. Three compounds associating for the first time polyoxotungstates, bisphosphonates and copper ions have been structurally characterized. They consist in heteropolyanionic monodimensional materials where $[Cu_6(Ale)_4(H_2O)_4]^{4-}$ (Ale = alendronate = $[O_3PC(O)(C_3H_6NH_3)PO_3]^{4-}$) complexes alternate with polyoxometalate (POM) units. In $Na_{12}[\{SiW_9O_{34}Cu_3(Ale)(H_2O)\}\{Cu_6(Ale)_4(H_2O)_4\}]\cdot 50H_2O$ (**SiW$_9$CuAle**), the polyoxometalate core consists in a $\{SiW_9Cu_3\}$ monomer capped by a pentacoordinated Ale ligand, while sandwich-type Keggin $\{(SbW_9O_{33})_2Cu_3(H_2O)_{2.5}Cl_{0.5}\}$ and Dawson $\{(P_2W_{15}O_{56})_2Cu_4(H_2O)_2\}$ complexes are found in $Na_8Li_{29}[\{(SbW_9O_{33})_2Cu_3(H_2O)_{2.5}Cl_{0.5}\}_2\{Cu_6(Ale)_4(H_2O)_4\}_3]\cdot 163H_2O$ (**SbW$_9$CuAle**) and $Na_{20}[\{(P_2W_{15}O_{56})_2Cu_4(H_2O)_2\}\{Cu_6(Ale)_4(H_2O)_4\}]\cdot 50H_2O$ (**P$_2$W$_{15}$CuAle**), respectively. A comparative magnetic study of the **SiW$_9$CuAle** and **SbW$_9$CuAle** compounds has allowed to fully quantify the Cu^{II} superexchange interactions either for the POM and non-POM subunits, evidencing that while the paramagnetic centers are antiferromagnetically coupled in the polyoxometalate units, both antiferromagnetic and ferromagnetic interactions coexist in the $\{Cu_6(Ale)_4(H_2O)_4\}$ cluster. All the studied compounds present a good efficiency upon the reduction of HNO_2 or NO_2^-, the POM acting as a catalyst. However, it has been found that **SbW$_9$CuAle** is inactive toward the reduction of nitrates, highlighting that both the $\{(SbW_9O_{33})_2Cu_3\}$ unit and the $\{Cu_6(Ale)_4(H_2O)_4\}$ cluster do not act as electrocatalysts for this reaction. In contrast, **SiW$_9$CuAle** and **P$_2$W$_{15}$CuAle** have shown a significant activity upon the reduction of NO_3^- and thus both at pH 1 and pH 5, evidencing that the chemical nature of the polyoxometalate is a crucial parameter even if it acts as pre-catalyst. Moreover, comparison of the activities of **P$_2$W$_{15}$CuAle** and $[(P_2W_{15}O_{56})_2Cu_4(H_2O)_2]^{16-}$ evidenced that if the $\{Cu_6(Ale)_4(H_2O)_4\}$ cluster do not act as electrocatalysts, it act as a co-factor, significantly enhancing the catalytic efficiency of the active POM.

Introduction

Among polyoxometalates (POMs),[1] polyoxotungstates (POTs) and especially the Dawson or Keggin type POT derivatives occupy a specific place as they represent perfect candidates for the multi-step elaboration of POM-based materials. In particular, starting from well-known vacant polyoxotungstate precursors[2] able to incorporate from one to twenty 3d centers, a vast family of 3d-incorporating inorganic compounds with a tremendous variety of compositions and structures has been obtained.[3] Organic-inorganic hybrid 3d metal-POTs have also been isolated using a large range of secondary oxygen ((poly)carboxylate)[4] and nitrogen (ethylenediamine, (poly)pyridine, azide,…)[5] containing ligands. As they represent a class of well-insulated complexes of controlled nuclearity and topology, these inorganic or hybrid materials constitute ideal models for magnetic investigations.[6] Moreover, these last years, several POM compounds behaving as Single-Molecule Magnets have been characterized.[7] 3d-containing polyoxotungstates have also been widely investigated for their catalytic and electrocatalytic properties.[8] For example, the ability of the $[Co^{II}_4(H_2O)_2(PW_9O_{34})_2]^{10-}$ complex to act as a robust water oxidation catalyst has been demonstrated.[9] The epoxidation of alkenes by Zn^{II}, Fe^{III} or Ni^{II}/Fe^{III} POTs has also been studied.[10] Besides, the electrocatalytic activity of these materials has been investigated, focusing mainly on the NOx reduction. Especially, a huge number of 3d-POTs have been found to reduce nitrites electrochemically.[11] In contrast, much less substituted POTs have been found to be active toward nitrate electroreduction. In short, it has been found that some POTs incorporating Cu^{II}[12] or Fe^{III}[13] centers can be highly active for the reduction of NO_3^-. More recently, it has been shown that a POT incorporating Ni^{II} centers and bisphosphonate (BP) ligands is also able to efficiently reduce nitrate into nitrogen.[14] Herein we report on a series of BP/POT/Cu^{II} compounds. The reactivity of three different vacant POTs ($[A\text{-}\alpha\text{-}SiW_9O_{34}]^{10-}$, $[\alpha\text{-}SbW_9O_{33}]^{9-}$ and $[\alpha\text{-}P_2W_{15}O_{56}]^{12-}$, respectively) with the $[O_3PC(OH)(C_3H_6NH_2)PO_3]^{4-}$ alendronate ligand (Ale) and Cu^{II} ions has been thoroughly

studied, and three new compounds structurally characterized. Surprisingly, they all contain chains built of two anionic fragments where POM units – the POM being purely inorganic or incorporating the alendronate ligand – and copper/alendronate multinuclear clusters alternate. The magnetic properties of two of these compounds have been thoroughly studied, allowing quantifying the magnetic exchange interactions both within the POM complexes and the copper/alendronate entities. The abilities of these three compounds to electrochemically reduce nitrites and nitrates have been evaluated and compared, highlighting that the nature of the POM plays a crucial role in the electrocatalytic activity even if these materials can act as pre-electrocatalysts since the reduction of the nitrate ions occurs at a potential lower than the one of the Cu(II/I) reduction. Also, the ability of the copper/alendronate entity to act as a co-factor is discussed.

Experimental section

Synthesis. All reagents were purchased and used without further purification except alendronic acid $H_4[O_3PC(OH)(C_3H_6NH_2)PO_3]$ (**Ale**),[15] $K_{12}[(SbW_9O_{33})_2\{Cu(H_2O)\}_3]\cdot 41H_2O$ (**$Sb_2W_{18}Cu_3$**),[16] $Na_{10}[A\text{-}\alpha\text{-}SiW_9O_{34}]\cdot xH_2O$ (**SiW_9**),[2] $Na_{12}[\alpha\text{-}P_2W_{15}O_{56}]\cdot 24H_2O$ (**P_2W_{15}**),[2] and $Na_9[\alpha\text{-}SbW_9O_{33}]\cdot 19.5H_2O$ (**SbW_9**),[17] which have been synthesized according to reported procedures.

Preparation of $Na_{12}[\{SiW_9O_{34}Cu_3(Ale)(H_2O)\}\{Cu_6(O_3PC(O)(C_3H_6NH_3)PO_3)_4(H_2O)_4\}]\cdot 50H_2O$ (**SiW_9CuAle**): $Na_{10}[\alpha\text{-}SiW_9O_{34}]\cdot nH_2O$ (500 mg, $1.78\ 10^{-4}$ mole (n = 20)) and $CuCl_2\cdot 2H_2O$ (121 mg, $7.09\ 10^{-4}$ mole) are dissolved in 10 mL of water and the pH adjusted to 7.5 with 1M NaOH. Then, alendronic acid (93 mg, $3.73\ 10^{-4}$ mole) is added and the pH readjusted to 7.5 with 1M NaOH. The solution is stirred for two hours at room temperature, and let slowly evaporating. After one week, green needle crystals suitable for X-Ray diffraction studies are collected and

washed with ethanol and ether (m = 250 mg; yield = 64% based on Ale). Anal. calc. (found) for $SiW_9O_{120}Cu_9C_{20}H_{147}N_5P_{10}Na_{12}$ (M. W. = 5218.4 g.mol^{-1}): W 31.71 (29.72), Cu 10.96 (11.06), P 5.93 (5.89), Na 5.29 (5.44), C 4.60 (4.64), H 2.84 (2.51), N 1.34 (1.18). IR (ν/cm^{-1}): 1626 (m), 1511 (m), 1472 (m), 1395 (w), 1109 (m), 1054 (s), 1115 (m), 980 (m), 967 (m), 950 (m), 930 (m), 911 (m), 878 (s), 804 (s), 671 (s), 559 (s), 509 (s).

Preparation of $Na_8Li_{29}[\{(SbW_9O_{33})_2Cu_3(H_2O)_{2.5}Cl_{0.5}\}_2\{Cu_6(O_3PC(O)(C_3H_6NH_3)PO_3)_4(H_2O)_4\}_3]\cdot 163\ H_2O$ (**SbW_9CuAle**): $Na_9[\alpha\text{-}SbW_9O_{33}]\cdot 19.5H_2O$ (570 mg, 2 10^{-4} mole) and alendronic acid (80 mg, 3.21 10^{-4} mole) are dissolved in 10 mL of water. Then

, $CuCl_2\cdot 2H_2O$ (108 mg, 6.33 10^{-4} mole) is added and the pH adjusted to 8 with 1M NaOH. The solution is stirred for one hour at room temperature. The addition of 750 mg of NaCl leads to the precipitation of a green powder which is redissolved in 20 mL of 1M LiCl. After one week, green needle crystals suitable X-Ray diffraction studies are collected and washed with ethanol and ether (m = 200 mg; yield = 43% based on Cu). Anal. calc. (found) for $Sb_4W_{36}Cu_{24}P_{24}C_{48}N_{12}H_{444}ClNa_8Li_{29}O_{396}$ (M. W. = 17322.5 g.mol^{-1}): W 38.21 (37.30), Cu 8.80 (8.82), P 4.29 (4.32), C 3.33 (3.41), H 2.58 (2.19), N 0.97 (0.93), Na 1.06 (1.00), Li 1.16 (1.13). IR (ν/cm^{-1}): 1625 (m), 1493 (m), 1396 (w), 1115 (m), 1049 (s), 932 (s), 864 (s), 682 (s), 566 (s), 505 (s).

Preparation of $Na_{20}[\{(P_2W_{15}O_{56})_2Cu_4(H_2O)_2\}\{Cu_6(O_3PC(O)(C_3H_6NH_3)PO_3)_4(H_2O)_4\}]\cdot 50H_2O$ (**$P_2W_{15}CuAle$**): $CuCl_2\cdot 2H_2O$ (60 mg, 4.46 10^{-4} mole) and alendronic acid (45 mg, 1.80 10^{-4} mole) are dissolved in 20 mL of water. Then, $Na_{12}[\alpha\text{-}P_2W_{15}O_{56}]\cdot 24H_2O$ (750 mg, 1.74 10^{-4} mole) is added as a solid and the pH adjusted to 7 with 1M NaOH. The solution is stirred for two hours at room temperature. Finally, NaCl (40 mg) is added and the solution is left to crystallize. After two weeks, green rod crystals suitable for X-Ray diffraction studies are collected and washed with ethanol and ether (m = 152 mg; yield = 32% based on Ale). Anal.

calc. (found) for $P_{12}W_{30}Cu_{10}C_{16}H_{148}N_4O_{196}Na_{20}$ (M. W. = 10515.4 g.mol^{-1}): P 3.53 (3.67), W 52.45 (50.07), Cu 6.04 (6.05), C 1.83 (2.10), H 1.42 (1.74), N 0.53 (0.53), Na 4.37 (4.28). IR (ν/cm^{-1}): 1622 (m), 1494 (m), 1395 (w), 1118 (m), 1081 (s), 1051 (s), 1015 (m), 933 (s), 877 (s), 727 (s), 687 (s), 577 (s), 558 (s).

Physical Measurements. Elemental analyses of the solids were performed by the "Service de microanalyses ICSN CNRS", in Gif sur Yvette (France), and by the "Service d'Analyse du CNRS", in Vernaison (France). FT-IR spectra were recorded in the 4000-400 cm^{-1} range on a Nicolet 30 ATR 6700 FT spectrometer. Single-crystal X-Ray intensity data collections were carried out with a Bruker Nonius X8 APEX 2 diffractometer equipped with a CCD bidimensional detector using Mo Kα monochromatized radiation (λ = 0.71073 Å). The absorption corrections were based on multiple and symmetry-equivalent reflections in the data sets using the SADABS program[18] based on the method of Blessing.[19] The structures were solved by direct methods and refined by full-matrix least-squares using the SHELX-TL package.[20] In the three reported structures, there is a discrepancy between the formulae determined by elemental analysis and that deduced from the crystallographic atom list because of the difficulty in locating all the disordered water molecules and alkali ions. Disordered water molecules and counter-ions were thus refined with partial occupancy factors. The hydrogen atoms were theoretically located on the basis of the conformation of the supporting atoms. The crystallographic data are gathered in Table 1. CCDC numbers: 1431904 (**SiW$_9$CuAle**), 1431905 (**SbW$_9$CuAle**) and 1431906 (**P$_2$W$_{15}$CuAle**).

Magnetic measurements. Magnetic measurements on powder were carried out with a Quantum Design SQUID Magnetometer with an applied field of 1000 G using powder samples pressed in pellets to avoid preferential orientation of the crystallites. The independence of the susceptibility value with regard to the applied field was checked at room temperature. The

susceptibility data were corrected from the diamagnetic contributions as deduced by using Pascal's constant tables. The susceptibility times temperature as a function of temperature curves have been simulated using MAGPACK.[21]

Electrochemistry. The solution were deaerated thoroughly for at least 30 minutes with pure argon and kept under a positive pressure of this gas during experiments.

Electrochemical measurements were carried out on a PARSTAT 2273 potentiostat at room temperature under argon atmosphere. A three-electrode system was used with a glassy carbon (GC, Tokai Japan) electrode as a working electrode, a platinum wire as auxiliary electrode and the reference electrode was the saturated calomel electrode, which was electrically connected to the solution by a junction bridge filled with electrolyte. The buffer solutions were prepared from the following solution, 1 mol.L^{-1} CH_3COOLi + CH_3COOH (pH 5) and 0.5 mol L^{-1} Na_2SO_4 + H_2SO_4 (pH 1).

Results and discussion

Synthesis and structures of SiW_9CuAle, SbW_9CuAle and $P_2W_{15}CuAle$. $Na_{12}[\{SiW_9O_{34}Cu_3(Ale)(H_2O)\}\{Cu_6(Ale)_4(H_2O)_4\}]\cdot 50H_2O$ (**SiW_9CuAle**) can be obtained in good yield (64%) in water (pH = 7.5) at room temperature from the reaction of [A-α-$SiW_9O_{34}]^{10-}$, $CuCl_2$ and alendronate. **SiW_9CuAle** results from the co-crystallization of two distinct polyanionic units, the polyoxometalate/copper/alendronate $[SiW_9O_{34}Cu_3(Ale)(H_2O)]^{8-}$ complex (Figure 1a) and the copper/alendronate $[Cu_6(Ale)_4(H_2O)_4]^{4-}$ cluster (Figure 1b). In **SiW_9CuAle**, all the alendronate ligands are tetraanionic, the global charge of the compound being compensated by twelve sodium cations. In the $\{SiW_9O_{34}Cu_3(Ale)(H_2O)\}$ POM, the 3d metal cations fill the vacancies of the $\{SiW_9\}$ precursor, the three Cu^{II} ions forming a pseudo-isosceles triangle ($d_{Cu\cdots Cu}$ = 3.67 and 3.84-3.85 Å respectively). Each paramagnetic center is connected to three oxygen atoms of the silicotungstate ligand and an alendronate ligand caps

the $\{SiW_9Cu_3\}$ fragment, connecting two copper ions of two edges of the triangle via one O-P-O bridges, respectively. In the third edge, the d^9 centers are directly connected via the deprotonated alkoxo group of the Ale ligand and via a long O-P-C-P-O bridge. All the 2p-orbitals of the Ale bridging oxygen atoms are directed toward the Cu^{II} $d_{x^2-y^2}$ magnetic orbitals. We can note that while the $[SiW_9O_{37}\{Cu(H_2O)\}_3]^{10-}$ species has been postulated,[22] it has not been possible so far to isolate this monomeric complex. However, several $\{SiW_9\}/Cu^{II}$ compounds have been characterized, including one monomeric $\{SiW_9Cu_4\}$ hybrid compound,[4f] four dimeric $\{(SiW_9)_2Cu_n\}$ (n = 5,[23] 6[24] or 8[25]) species and a tetrameric $\{(SiW_9)_4Cu_{14}\}$ complex.[26]

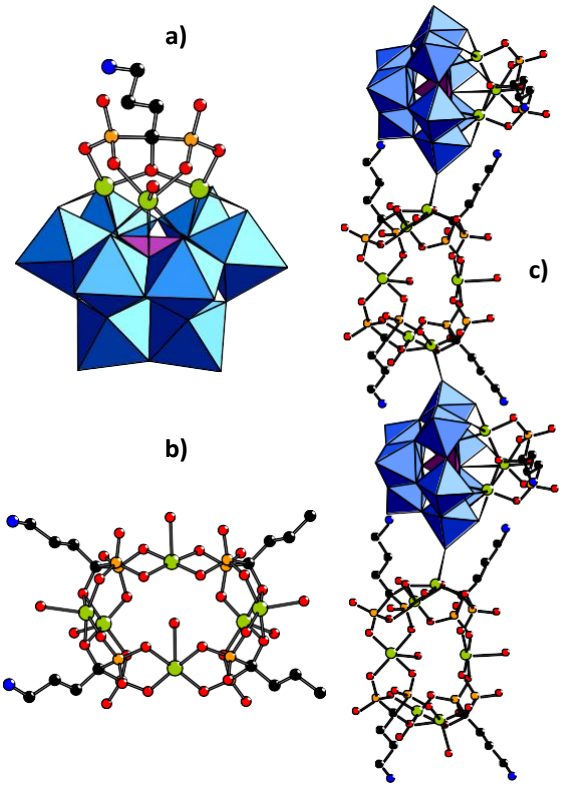

Figure 1. Ball and stick representations of a) the monomeric $\{SiW_9O_{34}Cu_3(Ale)(H_2O)\}$ Keggin building unit found in **SiW_9CuAle**; b) the $\{Cu_6(Ale)_4(H_2O)_4\}$ unit common to **SiW_9CuAle**, **SbW_9CuAle** and **$P_2W_{15}CuAle$** and c) the 1D structure of $[\{SiW_9O_{34}Cu_3(Ale)(H_2O)\}\{Cu_6(Ale)_4(H_2O)_4\}]^{12-}$. Blue octahedra, WO_6; purple tetrahedra, SiO_4; green spheres, Cu; orange spheres, P; black spheres, C; blue spheres, N; red spheres, O. Hydrogen atoms have been omitted for clarity.

Focusing now on the $[Cu_6(Ale)_4(H_2O)_4]^{4-}$ complex, it is observed that this unit contains two $\{Cu_2(Ale)_2(H_2O)_2\}$ pairs where all the copper atoms are in square pyramidal distorted environment. The basal planes of the copper ions are each made of two bridging alkoxo ligands ($d_{Cu\cdots O}$ = 1.93-1.99 Å, Cu-O-Cu = 88.8-90.1°) and two P-O oxygen atoms ($d_{Cu\cdots O}$ = 1.93-1.95 Å). These pairs are connected by two copper centers via eight O-P-O bridges, affording a cyclic hexanuclear species. Again, all the bridging oxygen atoms reside in the *xy* planes. While the coordination sphere of one Cu^{II} ion of each $\{Cu_2(Ale)_2(H_2O)_2\}$ pair is completed by a terminal water molecule ($d_{Cu\cdots O}$ = 2.36-2.37 Å), the other one is connected to a terminal O=W oxygen atom ($d_{Cu\cdots O}$ = 2.29-2.34 Å) of the $\{W_6\}$ crown of the $[SiW_9O_{34}Cu_3(Ale)(H_2O)]^{8-}$ moiety, affording a -POM-$\{Cu_6\}$-POM-$\{Cu_6\}$- infinite molecular wire (Figure 1c). It can be noticed that only one pure alendronate/copper cluster has been previously fully characterized,[27] and its structure is completely different from that of the $[Cu_6(Ale)_4(H_2O)_4]^{4-}$ one found in **SiW_9CuAle**. Indeed, in the neutral dinuclear $[Cu_2(Ale)_4(H_2O)_2]$ complex previously reported, the copper centers are connected by two Ale ligands via two O-P-O and two O-P-C-P-O bridges, all the alkoxo groups of the Ale ligands remaining protonated. This can be explained considering the much lower pH (pH = 2) of the reacting media compared to the one fixed for the synthesis of **SiW_9CuAle** (pH = 7.5). The IR spectrum of **SiW_9CuAle** shows intense O-P-O symmetric and asymmetric stretching bands in the 1000-1200 cm^{-1} region. Above 1200 cm^{-1}, the bands related to the organic backbone are observed, while the intense bands due to the W=O and W-O vibrations are observed below 1000 cm^{-1}. **SiW_9CuAle** is soluble in water. It can be recovered after dissolution by addition of NaCl, the obtained product possessing exactly the same IR spectrum as the pristine one, strongly suggesting that both the $\{SiW_9O_{34}Cu_3(Ale)(H_2O)\}$ and the $\{Cu_6(Ale)_4(H_2O)_4\}$ fragments are stable in solution.

$Na_8Li_{29}[\{(SbW_9O_{33})_2Cu_3(H_2O)_{2.5}Cl_{0.5}\}_2\{Cu_6(Ale)_4(H_2O)_4\}_3]\cdot 163H_2O$ (**SbW_9CuAle**) has been obtained my mixing $[\alpha\text{-}SbW_9O_{33}]^{9-}$, $CuCl_2$ and Ale in water (room temperature, pH = 8).

Addition of NaCl afforded a precipitate which can be recrystallized in a 1M LiCl aqueous solution, leading to a mixed Na/Li salt. In **SbW$_9$CuAle**, one $[(SbW_9O_{33})_2Cu_3(H_2O)_2Cl]^{13-}$ and one $[(SbW_9O_{33})_2Cu_3(H_2O)_3]^{12-}$ POM units (Figure SI1) co-crystallize with three crystallographically independent $[Cu_6(Ale)_4(H_2O)_4]^{4-}$ complexes analogous to that found in **SiW$_9$CuAle**. The $\{Sb^{III}_2W_{18}Cu_3\}$ POM cluster has been previously described[16] and consists in three Cu^{II} centers sandwiched between two $\{Sb^{III}W_9\}$ units and connected via long O-W-O-W-O bridges ($d_{Cu\cdots Cu}$ = 4.72-4.84 Å). As for the **SiW$_9$CuAle** compound, two copper centers of each $[Cu_6(Ale)_4(H_2O)_4]^{4-}$ cluster are connected to O=W oxygen atoms ($d_{Cu\cdots O}$ = 2.17-2.31 Å) of the $\{W_6\}$ crown of the POM. However, in opposition to **SiW$_9$CuAle**, in **SbW$_9$CuAle**, the anionic units form a -POM-$\{Cu_6\}$-POM-$\{Cu_6\}_2$-POM-$\{Cu_6\}$-POM-$\{Cu_6\}_2$- chain (Figure 2a), with a POM:$[Cu_6(Ale)_4(H_2O)_4]^{4-}$ ratio of 2:3 compared to 1:1 in **SiW$_9$CuAle**.

The third compound $Na_{20}[\{(P_2W_{15}O_{56})_2Cu_4(H_2O)_2\}\{Cu_6(Ale)_4(H_2O)_4\}]\cdot 50H_2O$ (**P$_2$W$_{15}$CuAle**) has been synthesized in conditions similar to those used for **SiW$_9$CuAle** but replacing the $\{SiW_9\}$ precursor with the $\{P_2W_{15}\}$ one. **P$_2$W$_{15}$CuAle** is made of the $[(P_2W_{15}O_{56})_2Cu_4(H_2O)_2]^{16-}$ POM, which can be described as a rhomb-like tetranuclear Cu^{II} cluster sandwiched between two $\{P_2W_{15}\}$ units,[28] and of the $[Cu_6(Ale)_4(H_2O)_4]^{4-}$ complex. In the solid state, $[(P_2W_{15}O_{56})_2Cu_4(H_2O)_2]^{16-}$ clusters alternate with $[Cu_6(Ale)_4(H_2O)_4]^{4-}$ units, forming a -POM-$\{Cu_6\}$-POM-$\{Cu_6\}$- 1D material (Figure 2b), the $[Cu_6(Ale)_4(H_2O)_4]^{4-}$ complexes and the POMs being connected via oxygen atoms belonging to the $\{W_3\}$ caps of the Dawson units ($d_{Cu\cdots O}$ = 2.21-2.23 Å). Finally, to date, attempts to isolate separately the POM and the $\{Cu_6Ale_4\}$ clusters by adding various counter-cations to an aqueous solution of **SbW$_9$CuAle** have failed, a combination of the two anionic species exhibiting an IR spectrum strictly analogous to that of **SbW$_9$CuAle** being systematically obtained.

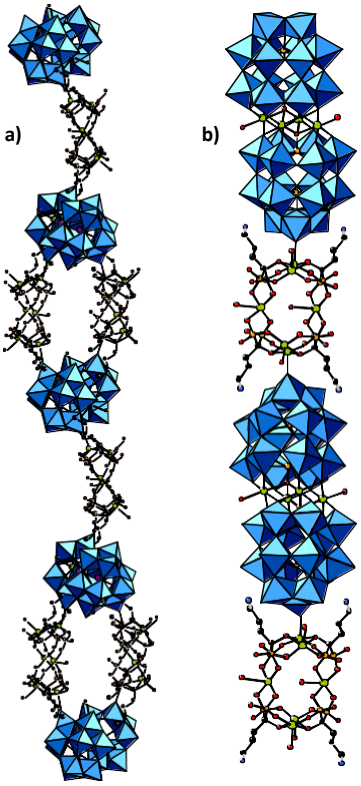

Figure 2. Ball and stick representations of the 1D structures of a) $[\{(SbW_9O_{33})_2Cu_3(H_2O)_{2.5}Cl_{0.5}\}_2\{Cu_6(Ale)_4(H_2O)_4\}_3]^{37-}$ (**SbW₉CuAle**) and b) $[\{(P_2W_{15}O_{56})_2Cu_4(H_2O)_2\}\{Cu_6(Ale)_4(H_2O)_4\}]^{20-}$ (**P₂W₁₅CuAle**). Blue octahedra, WO_6; purple spheres, Sb; green spheres, Cu; orange spheres, P; black spheres, C; blue spheres, N; red spheres, O.

Magnetic properties. The magnetic properties of **SbW₉CuAle** and **SiW₉CuAle** have been investigated, and the $\chi_M T$ product vs. T curves of powdered samples of these compounds are represented on Figures 3a and 4a, respectively. For **SbW₉CuAle**, $\chi_M T$ continuously decreases from 300 K ($\chi_M T$ = 10.98 $cm^3.mol^{-1}.K$, the $\chi_M T$ value calculated for 24 non-interacting Cu^{II} centers being 10.89 $cm^3.mol^{-1}.K$ assuming g = 2.2) to 2 K ($\chi_M T$ = 6.82 $cm^3.mol^{-1}.K$), indicating that overall weak antiferromagnetic interactions are predominant. In contrast, the $\chi_M T$ = f(T) curve related to **SiW₉CuAle** is characteristic of overall strong antiferromagnetic interactions, $\chi_M T$ decreasing from 300 K ($\chi_M T$ = 3.57 $cm^3.mol^{-1}.K$, the $\chi_M T$ value calculated for 9 non-interacting Cu^{II} centers being 4.08 $cm^3\ mol^{-1}\ K$ assuming g = 2.2) to 20 K ($\chi_M T$ = 3.20 $cm^3.mol^{-1}.K$). At low temperature, the $\chi_M T$ product increases from 20 K to 4 K ($\chi_M T$ = 3.38 $cm^3.mol^{-1}.K$), highlighting the presence of weak ferromagnetic interactions. Finally, $\chi_M T$ decreases from 4 to 2 K ($\chi_M T$ = 3.30 $cm^3.mol^{-1}.K$).

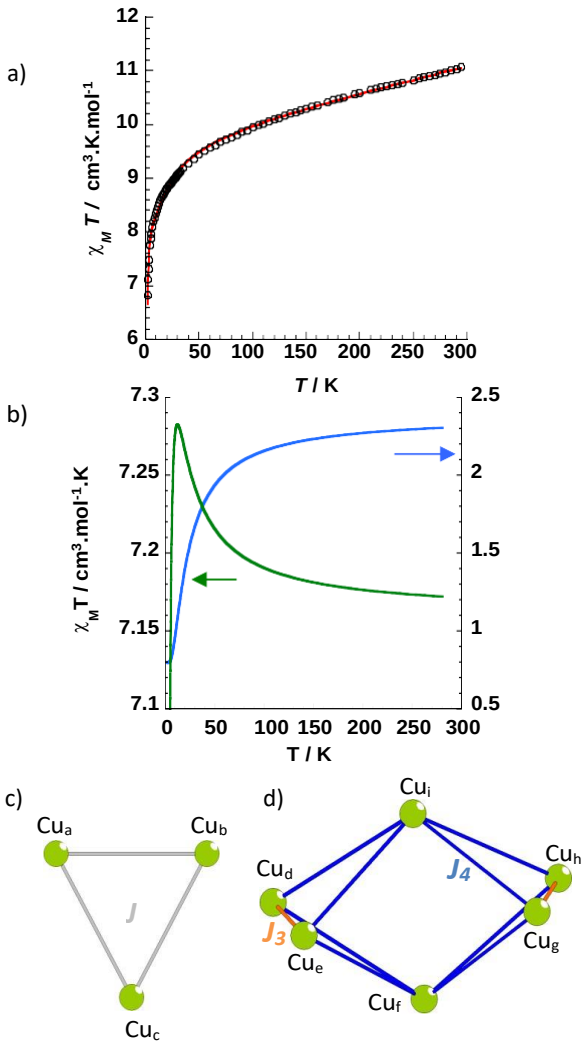

Figure 3. a) Thermal behaviour of $\chi_M T$ for **SbW$_9$CuAle** at 1000 Oe in the 2 – 300 K range. The solid red line above the experimental data is the theoretical curve derived from the Hamiltonian 1 (see text); b) deconvolution of the theoretical thermal behaviour of $\chi_M T$ for **SbW$_9$CuAle** highlighting the contributions of the POM (blue) and {Cu$_6$Ale$_4$} (green) fragments; c) the coupling scheme used for modelizing the magnetic behaviour of the {(SbW$_9$O$_{33}$)$_2$Cu$_3$} units in **SbW$_9$CuAle**; d) the coupling scheme used for modelizing the magnetic behaviour of the {Cu$_6$(Ale)$_4$(H$_2$O)$_4$} units in **SbW$_9$CuAle** and **SiW$_9$CuAle**.

The quantification of the magnetic exchange interactions in **SbW$_9$CuAle** and **SiW$_9$CuAle** is not an easy task considering that for these materials the measured $\chi_M T$ products are the resultant of the contributions of trinuclear POM units and hexanuclear {Cu$_6$Ale$_4$} BP complexes. Moreover, **SbW$_9$CuAle** is made of three crystallographically independent {Cu$_6$Ale$_4$} fragments and two crystallographically independent POM units (see above). Nevertheless, attempts to fit the data have been effectuated.

Starting with **SbW_9CuAle**, it has been considered that (i) the two POMs and the three $\{Cu_6Ale_4\}$ units constituting this material are magnetically equivalent, respectively and (ii) the $\{Cu_6Ale_4\}$ and the $\{(SbW_9)_2Cu_3\}$ units are magnetically isolated. Also, in the $\{(SbW_9)_2Cu_3\}$ fragment, it has been assumed that the copper centers form an equilateral triangle. Besides, a two-*J* model has been used for the modelization of the $\{Cu_6Ale_4\}$ complex. This led to the coupling schemes represented on Figures 3c and 3d, which correspond to the following Hamiltonian:

$$\hat{H}(1) = -2J(\hat{S}_{Cua}\hat{S}_{Cub} + \hat{S}_{Cub}\hat{S}_{Cuc} + \hat{S}_{Cuc}\hat{S}_{Cua}) - 2J_3(\hat{S}_{Cud}\hat{S}_{Cue} + \hat{S}_{Cug}\hat{S}_{Cuh}) - 2J_4(\hat{S}_{Cue}\hat{S}_{Cuf} + \hat{S}_{Cud}\hat{S}_{Cuf} + \hat{S}_{Cuf}\hat{S}_{Cug} + \hat{S}_{Cuf}\hat{S}_{Cuh} + \hat{S}_{Cug}\hat{S}_{Cui} + \hat{S}_{Cuh}\hat{S}_{Cui} + \hat{S}_{Cui}\hat{S}_{Cud} + \hat{S}_{Cui}\hat{S}_{Cue}) \quad (1)$$

A good fit to the experimental $\chi_M T$ data in the 300 – 2 K temperature range has been obtained for J = -6.80 cm^{-1}, J_3 = +2.40 cm^{-1} and J_4 = -0.37 cm^{-1} (TIP = 231 10^{-6} $cm^3.mol^{-1}$ per Cu^{II} center, g = 2.06 and R = 3.3 10^{-5}).[29] The calculated | J | value is slightly higher than those previously determined for pure $\{(XW_9)_2Cu_3\}$ (X = As, Sb, Ge) POM species.[30] This can be due to the approximations mentioned above. In particular, in **SbW_9CuAle**, the intramolecular Cu···Cu distances are in the 4.72-4.84 Å range, while the shortest Cu···Cu distances between the copper ions of the $\{(SbW_9)_2Cu_3\}$ and those of the $\{Cu_6Ale_4\}$ units are of 5.52 Å. These relatively short intermolecular copper-copper distances can induce weak interactions, not taken into account in our model.

Focusing now on the $\{Cu_6Ale_4\}$ cluster, it is found that both ferromagnetic and antiferromagnetic magnetic interactions coexist in this fragment. It is well known that while several parameters affect the amplitude of the magnetic interactions in $\{Cu(OX)_2Cu\}$ (X = H, CH_3, Ph...) dimers with $d_{x^2-y^2}$ copper orbitals directed toward the bridging ligands, the major factor controlling the exchange coupling is the Cu-O(X)-Cu θ bridging angle. In OH-bridged complexes, based both on experimental results[31] or theoretical calculations,[32] a linear correlation between J and θ has been proposed, with a crossover point at $\theta \sim 97.5°$ below which

the magnetic behaviour changes from antiferromagnetic to ferromagnetic coupling. In contrast, for OPh-bridged complexes a crossover point has been theoretically predicted at $\theta \sim 77.5°$,[33] highlighting the huge importance of the X substituent borne by the oxygen atom. In the $\{Cu_6Ale_4\}$ cluster, the Cu_d and Cu_e and the Cu_h and Cu_g centers are dibridged by oxygen atoms of {P-C(O)-P} BP groups, respectively. Such magnetic core has not been previously reported. However it can be mentioned that the $\{Cu\text{-}O(CP_2)\text{-}Cu\}$ fragment is characterized by θ angles in the 87.8-90.6° range. Such very low bridging angles must highly favour ferromagnetic interactions. Also, the two connected $\{CuO_4\}$ fragments are not planar, with a dihedral angle of 65.2-66.9°, thus reducing the overlap of the magnetic orbitals of the copper centers via the p-orbitals of the bridging oxygens. Both these factors explain the sign of the $J_3 = +2.40$ cm^{-1} constant determined.[34] Finally, weak antiferromagnetic interactions ($J_4 = -0.37$ cm^{-1}) have been found between the copper centers connected by {O-P-O} bridges. The energy diagram deduced from the J_3 and J_4 values indicate that the ground state characterizing $\{Cu_6Ale_4\}$ is a triplet, with a $S = 0$ first excited state very close in energy and located at 0.74 cm^{-1}. The magnetic behavior of **SiW_9CuAle** has been interpreted considering the POM $\{SiW_9Cu_3\}$ fragment and the $\{Cu_6Ale_4\}$ cluster as magnetically isolated. In $\{SiW_9Cu_3\}$, the copper centers form an isosceles triangle, necessitating the introduction of an additive exchange parameter compared to the model used for the $\{SbW_9Cu_3\}$ magnetic unit. The coupling scheme associated to **SiW_9CuAle** is represented on Figures 3d and 4c, and leads to the following Hamiltonian:

$$\hat{H}(2) = -2J_1\hat{S}_{Cua}\hat{S}_{Cub} - 2J_2(\hat{S}_{Cub}\hat{S}_{Cuc} + \hat{S}_{Cuc}\hat{S}_{Cua}) - 2J_3(\hat{S}_{Cud}\hat{S}_{Cue} + \hat{S}_{Cug}\hat{S}_{Cuh}) - 2J_4(\hat{S}_{Cue}\hat{S}_{Cuf} + \hat{S}_{Cud}\hat{S}_{Cuf} + \hat{S}_{Cuf}\hat{S}_{Cug} + \hat{S}_{Cuf}\hat{S}_{Cuh} + \hat{S}_{Cug}\hat{S}_{Cui} + \hat{S}_{Cuh}\hat{S}_{Cui} + \hat{S}_{Cui}\hat{S}_{Cud} + \hat{S}_{Cui}\hat{S}_{Cue}) \quad (2)$$

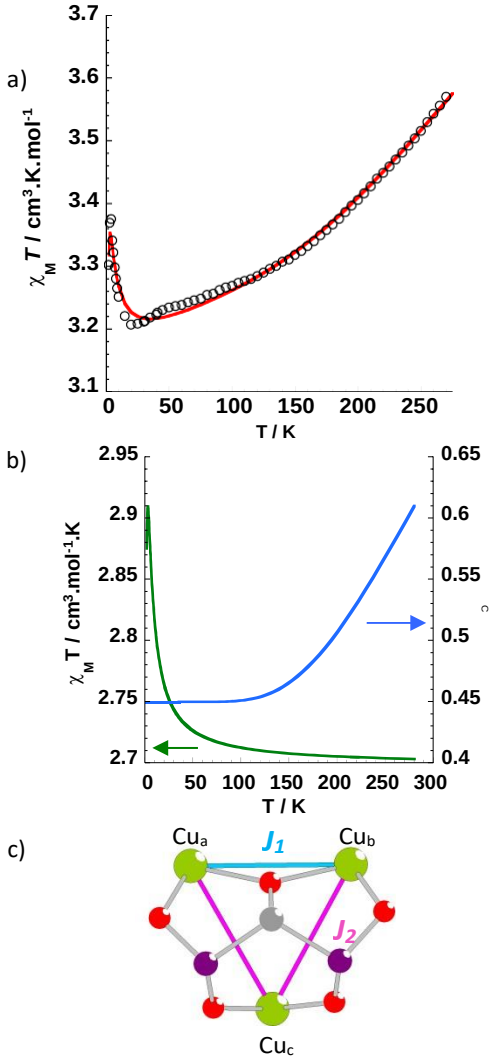

Figure 4. a) Thermal behaviour of $\chi_M T$ for **SiW$_9$CuAle** at 1000 Oe in the 2 – 300 K range. The solid red line above the experimental data is the theoretical curve derived from the Hamiltonian 2 (see text); b) deconvolution of the theoretical thermal behaviour of $\chi_M T$ for **SiW$_9$CuAle** highlighting the contributions of the POM (blue) and {Cu$_6$Ale$_4$} (green) fragments. c) the coupling scheme used for modelizing the magnetic behaviour of the {SiW$_9$O$_{34}$Cu$_3$(Ale)(H$_2$O)}unit in **SiW$_9$CuAle**.

The best fit to the experimental $\chi_M T$ data in the 300 – 2 K temperature range has been obtained for J_1 = -255 cm^{-1}, J_2 = -55.0 cm^{-1}, J_3 = +1.56 cm^{-1} and J_4 = -0.11 cm^{-1} (TIP = 110 10^{-6} cm^3.mol^{-1} per Cu^{II} center, g = 2.19 and R = 8.6 10^{-6}).[29] Considering the {SiW$_9$Cu$_3$} fragment, the $d_{x^2-y^2}$ orbitals of the Cu$_a$ and Cu$_b$ atoms interact via the p-orbital of the deprotonated O(C) atom of the BP ligand, with a low dihedral angle of 12.1° and a large θ Cu-O-Cu bridging angle of 134.1°. This leads to a strong antiferromagnetic interaction (J_1 = -255 cm^{-1}), slightly higher than

those found for the few previously reported single alkoxo-bridged Cu^{II} dimers. For example, a coupling constant of -191.5 cm^{-1} has been found for the $[Cu_2(bdmap)(acac)(NH_3)]^{2+}$ (bdmap = 1,3-bis(dimethylamino)-2-propanolato; acac = acetylacetonate) complex (θ =135.8°).[35] However, in **SiW_9CuAle**, the copper centers are bridged by an additional O-Si-O groups. The coupling constant associated with the interactions involving the magnetic metal centers connected via O-P-O bridges is also negative, but as expected weaker (J_2 = -55.0 cm^{-1}).

While the $\chi_M T$ behaviour at high temperature is mainly due to the $\{SiW_9Cu_3\}$ unit, at lower temperature, the increase observed between 25 and 3 K is related to the ferromagnetic interactions between respectively the Cu_d and Cu_e and the Cu_h and Cu_g centers (J_3 = +1.56 cm^{-1}) belonging to the $\{Cu_6Ale_4\}$ fragment (Figure 4b). In contrast, we can note that for **SbW_9CuAle**, the low temperature $\chi_M T$ vs. T behaviour is due *both* to the $\{Cu_6Ale_4\}$ (J_3 = +2.40 cm^{-1} and J_4 = -0.37 cm^{-1}) and the $\{SiW_9Cu_3\}$ (J = -6.80 cm^{-1}) fragments. As a consequence, on the **SbW_9CuAle** $\chi_M T$ *vs.* T plot, the ferromagnetic coupling in $\{Cu_6Ale_4\}$ is masked by the weak antiferromagnetic coupling in the $\{SbW_9Cu_3\}$ fragment; a deconvolution of the $\chi_M T$ vs. T curve is thus needed for visualizing the ferromagnetic exchange in **SbW_9CuAle** (Figure 3b). In addition, for **SiW_9CuAle,** the $\chi_M T$ decrease below 3K is correlated to the small antiferromagnetic interactions between the O-P-O bridged Cu^{II} ions of $\{Cu_6Ale_4\}$ (J_4 = -0.11 cm^{-1}). Importantly, we can note that the magnetic coupling constants characterizing the $\{Cu_6Ale_4\}$ unit and determined in **SbW_9CuAle** and **SiW_9CuAle** are in good agreement.

Electrochemistry. The redox potentials of **$P_2W_{15}CuAle$**, **SbW_9CuAle** and **SiW_9CuAle** in a pH 5 and pH 1 medium are gathered in Table 2 and compared to that of the previously reported fully inorganic $[(SbW_9O_{33})_2\{Cu(H_2O)\}_3]^{12-}$ (**$Sb_2W_{18}Cu_3$**) POM[16] considered here as a reference.

The cyclic voltammogram (CV) of **$P_2W_{15}CuAle$** in a pH 5 medium is shown in Figure 5A. In the potential domain explored, it consists of three waves with peaks potential located at -0.14, -0.18 and -0.57 V *vs.* SCE, respectively. The last reversible wave, denoted III in Figure 5A, is attributed to the redox processes of the W centers (W^{VI}/W^{V} couple). To the reduction waves I and II is associated a single oxidation peak at -0.02 V *vs.* SCE with a characteristic shape usually encountered for the oxidation of Cu^0 species.[24b]

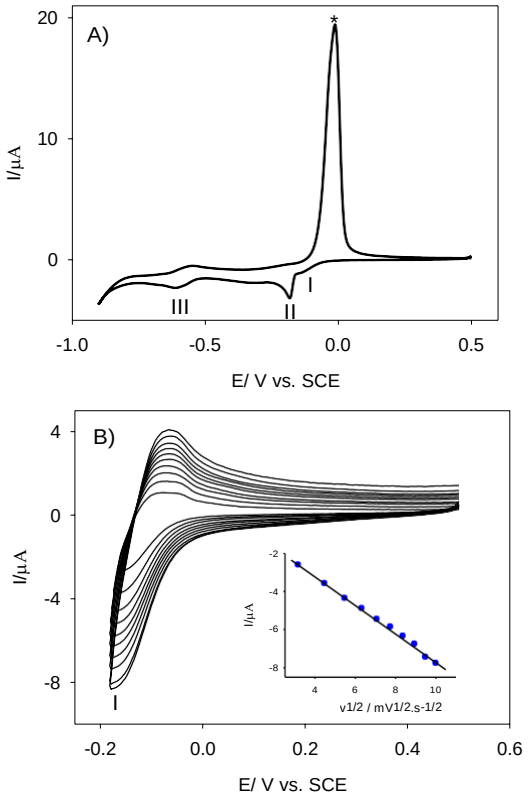

Figure 5. A) Cyclic voltammogram of 0.1 mM **$P_2W_{15}CuAle$** in a pH 5 buffer solution (1 M CH_3COOLi + CH_3COOH). v = 2 mV.s^{-1}. B) Variation of scan rates (from inner to outer curve) : 10, 20, 30, 40, 50, 60, 70, 80, 90, and 100 mV s^{-1}. The potential reversal is fixed after the Cu^{II} to Cu^{I} redox process. (Inset) Variation of the cathodic peak current intensity as a function of the square root of the scan rate. The working electrode was glassy carbon, and the reference electrode was the Saturated Calomel Electrode (SCE). * Reoxidation peak of the deposited Cu^0 on electrode surface.

The shapes and potential positions of the Cu^{II} reduction waves I and II are analogous to those already observed for Cu substituted POMs.[36] This pattern features the two-step reduction of Cu^{II} to Cu^0 through Cu^{I}. The first reduction wave is reversible. Plot of the cathodic current (I_{pc}) *vs.* the square root of the scan rate $v^{1/2}$ shows a linear dependence (inset of Figure 5B) showing

that the current is limited by the diffusion of **$P_2W_{15}CuAle$** to the electrode surface as expected for a reversible process where the species is in solution. Controlled potential coulometry at a potential just below that of the peak potential of the second reduction process of **$P_2W_{15}CuAle$** (at -0.20 V *vs.* SCE) indicates the exchange of 19 electrons per molecule, in agreement with the reduction of the 10 Cu^{II} centers in Cu^0. This is also confirmed by the black deposit visible on the electrode surface.

$Sb_2W_{18}Cu_3$, **SbW_9CuAle**, **SiW_9CuAle** and **$P_2W_{15}Cu_4$** show at pH 5 (see SI, Figures SI2-6) similar redox behaviour with two successive reduction waves associated to the reduction of Cu^{II} to Cu^{I} and the reduction of Cu^{I} to Cu^0. On potential reversal, a large oxidation current wave is observable which display the characteristic shape for the reoxidation of deposited Cu^0 on the electrode surface. Again for the first couple, Cu^{II}/Cu^{I}, the cathodic peak current (i_{pc}) is proportional to the square root of the scan rate which indicates that the electrochemical processes are diffusion controlled. For the compound **$P_2W_{15}Cu_4$** the first redox waves attributed to the W^{VI}/W^{V} couple is observed nearly at the same potential than for **$P_2W_{15}CuAle$** (Table 2) At variance, for **SbW_9CuAle** and **SiW_9CuAle**, the W^{VI}/W^{V} reversible waves III are not observable while two ill-defined waves are observed at -0.59 V and -0.81 V *vs.* SCE for the parent compound **$Sb_2W_{18}Cu_3$**. Controlled potential coulometry at a potential just below the peak potential of the second reduction process for **$Sb_2W_{18}Cu_3$**, **SbW_9CuAle** and **SiW_9CuAle** indicate that all the Cu^{II} centers are actually reduced with the exchange of 6.1, 48.2 and 18.2 electrons per molecule respectively.

At pH 1 all the compounds present similar redox behaviour with again two consecutive reduction waves related to the reduction of Cu^{II} to Cu^{I} and the reduction of Cu^{I} to Cu^0 (see ESI, Figures SI6-10). In the reverse scan, a large reoxidation current wave is still noticeable. The only change is a small anodic shift of ca. 70-80 mV for the Cu^{II}/Cu^{I} couple and of ca. 50-100 mV for the Cu^{I}/Cu^0 couple, showing that these compounds are easier to reduce at lower pH.

These small shifts may be due to the nature of the buffer used (1 M CH_3COOLi + CH_3COOH at pH 5 *vs.* 0.5 M Na_2SO_4 + H_2SO_4 at pH 1). Another possible explanation is the influence of the pK_a of the aqua Cu(II) centers (Cu^{II}-OH_2) that can be easily deprotonated, giving the hydroxo forms Cu(II) centers (Cu^{II}-OH) when the pH increases as shown in previous work.[37]

Electrocatalysis of NO_x reduction. Nitrate reduction was chosen to investigate the electrocatalytic capacities of each complex studied in this work. The nitrite reduction, NO_2^- being a possible chemical intermediate in the reduction of nitrate, has also been studied.

Reduction of Nitrate. The CVs were measured as a function of the excess parameter γ (γ = $C_{NO_3^-}/C_{POM}$) with the same potential scan rate (2 $mV.s^{-1}$). As is apparent in Figure 6 at pH 5 for **$P_2W_{15}CuAle$**, the addition of even modest quantities of nitrate induced a large cathodic current enhancement starting at a potential below -0.75 V (only after the first W wave). These observations show an efficient reduction of nitrate by the reduced species of **$P_2W_{15}CuAle$**. In the explored potential domain, no reduction of nitrate could be detected on the glassy carbon electrode in the absence of polyoxometalate complexes (see SI, Figure SI11). The relative electrocatalytic activities of the reported POMs can be determined calculating the kinetic current $J_{kinetic\ (NO_3^-)}$, using the following formula:

$$J_{kinetic\ (NO_3^-)} = (I_{POM+NO_3^-} - I_{POM})/S$$

where $I_{POM+NO_3^-}$ is the reduction current of the POM in the presence of nitrate, I_{POM} the reduction current for the POM alone and S the geometrical surface of the electrode. In the current experiment, for **$P_2W_{15}CuAle$** and at pH 5, the $J_{kinetic\ (NO_3^-)}$ measured at -0.90 V are -43.0 and -100.0 $\mu A.cm^{-2}$ for excess parameters γ ($\gamma = C^0_{NO_3-}/C^0_{POM}$) of 10 and 30, respectively.

SiW$_9$CuAle, in the same conditions, provides the $J_{kinetic\ (NO_3^-)}$ values of -99.2 and -209.6 $\mu A.cm^{-2}$ for γ = 10 and 30, respectively (see SI, Table SI1 and Figure SI12).

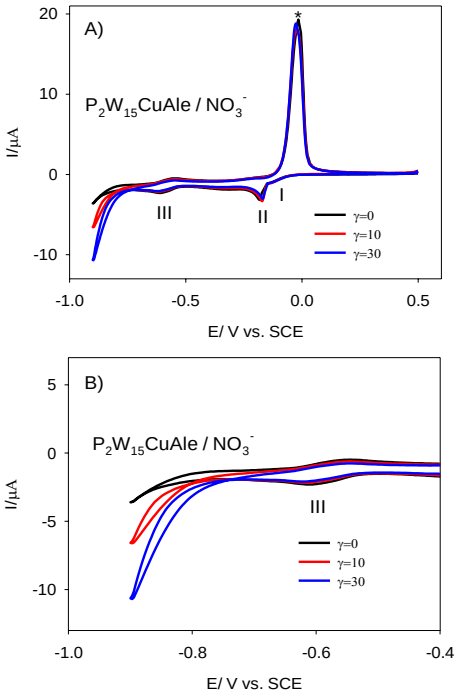

Figure 6. A) Electrocatalysis of NO_3^- reduction in the presence of 0.1 mM **P$_2$W$_{15}$CuAle** in a pH 5 medium, v = 2 mV.s^{-1}. B) Magnification of A) to highlight the reduction of nitrate ions. * Reoxidation peak of the deposited Cu^0 on electrode surface.

For **P$_2$W$_{15}$Cu$_4$**, using the same conditions at pH 5, the $J_{kinetic\ (NO_3^-)}$ measured at -0.90 V are lower: –8.7 and –22.7 $\mu A.cm^{-2}$ for excess parameters γ ($\gamma = C^0_{NO_3-}/C^0_{POM}$) of 10 and 30, respectively (see SI, Table SI1, Figures SI13-14). Similar electrocatalytic behavior were previously published by Nadjo et al. for this compound.[38] It thus should be noticed that the $J_{kinetic\ (NO_3^-)}$ obtained for **P$_2$W$_{15}$CuAle** are significantly higher than the ones obtained for the corresponding POM without the alendronate complexes, which might be due to the higher number of Cu atoms in the **P$_2$W$_{15}$CuAle** compound (4 in **P$_2$W$_{15}$Cu$_4$** versus 10 in **P$_2$W$_{15}$CuAle**).

Surprisingly, the compounds **Sb$_2$W$_{18}$Cu$_3$** and **SbW$_9$CuAle** do not present significant cathodic enhancements upon the addition of nitrate in solution (see SI, Table SI1, Figures SI15-16). In

contrast, **$P_2W_{15}CuAle$**, **$P_2W_{15}Cu_4$** and **SiW_9CuAle**, show an efficient reduction of nitrate but only after the first W wave of the POM subunit, and after the step II (couple Cu^I/Cu^0) corresponding to the copper deposition on the glassy carbon electrode. This suggests that the chemical nature of the POM entities adsorbed on the surface of the Cu^0 nanoparticles strongly affects the electrocatalytic activity for the reduction of nitrate on the Cu^0 nanoparticles.

Furthermore, it is worth pointing out that the catalytic current with Cu-containing polyoxometalates may not be due solely to the amount of deposited Cu^0 (which is higher for **SbW_9CuAle** than for **$P_2W_{15}CuAle$)**, but should also be influenced by the type of POM used. Thus the electrocatalytic reduction of nitrate must be traced successively to the properties of the electrodeposited copper and to those of the reduced W centres.

At pH 1, **$P_2W_{15}CuAle$** gives the $J_{kinetic\ (NO_3^-)}$ values of -145.3 and -397.5 $\mu A.cm^{-2}$ for γ = 10 and 30, respectively, showing an increase of current of the reduction of the nitrate at low pH (see SI, Figure SI17). **SiW_9CuAle** under the same conditions provides the same behaviour with $J_{kinetic\ (NO_3^-)}$ values of -276.5 and -537.0 $\mu A.cm^{-2}$ for γ = 10 and 30, respectively, indicating an increase of more than two times of the current for the reduction of nitrate for **SiW_9CuAle** at low pH (see SI, Table SI1, and Figure SI18). Again, **$Sb_2W_{18}Cu_3$** and **SbW_9CuAle** do not present a cathodic enhancement upon the addition of nitrate in solution at pH 1 (see SI, Table SI1 and Figures SI19 and SI20).

Reduction of Nitrite. All the four complexes have shown a good efficiency upon the reduction of nitrite. The results for $J_{kinetic\ (HNO_2/NO_2^-)}$ values are gathered for comparison in the Supporting Information (Table SI1, Figures SI21-28). Figure 7 indicates that upon reduction, **$P_2W_{15}CuAle$** catalyses the reduction of nitrite at pH 5.

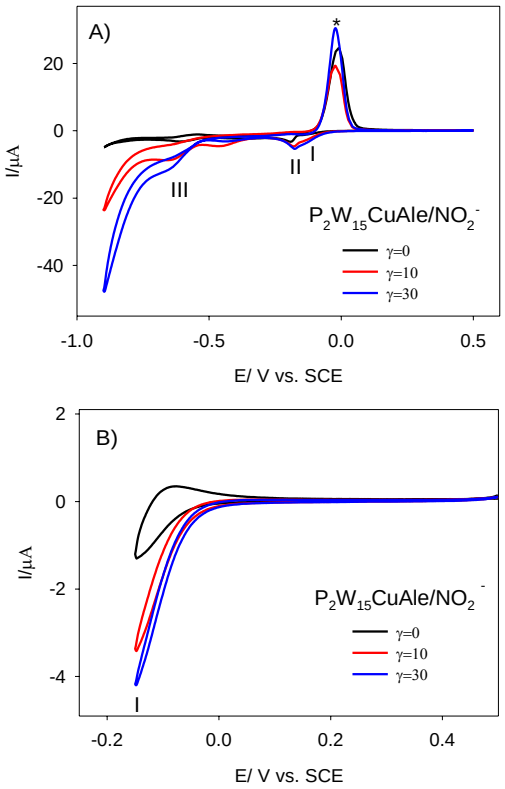

Figure 7. A) Electrocatalysis of NO_2^- reduction in the presence of 0.1mM **$P_2W_{15}CuAle$** in a pH 5 medium. v = 2 $mV.s^{-1}$, the working electrode was glassy carbon and the reference electrode was the Saturated Calomel Electrode (SCE). B) Electrocatalysis of NO_2^- reduction with reversal potential fixed after the Cu^{2+}/Cu^+ redox process. *Reoxydation peak of the deposited Cu^0 on electrode surface.

The electrocatalytic reduction of nitrite is found to occur just before the deposition of Cu^0 (wave II), already at the first reversible process of the reduction of Cu^{II}/Cu^{I} (wave I). $J_{kinetic\ (NO_2^-)}$ measured at -0.15 V (peak I) and for γ = 10 and 30 were -30.3 and -40.7 $\mu A.cm^{-2}$, respectively (see SI, Table SI1). In contrast, at this potential and in the same medium, no significant electrocatalytic activity toward the reduction of NO_3^- was detected. It is remarkable that in the presence of NO_2^-, a significant reduction current is obtained at the potential of the peak I, while no Cu^0 oxidation peak is obtained during the reversed anodic scan when the cathodic potential limit is set at -0.1 V *vs.* SCE (Figure 8B). This shows that the NO_2^- is able to reoxidize the electrochemically generated Cu^{I}POMAle species, leading to the regeneration of the Cu^{II}POMAle species which seem to be stable when the potential is kept above -0.1 V *vs.* SCE. It can be concluded that this POM is a good electrocatalyst for the reduction of nitrite in more acidic solution. We can note that at pH 1, the active species should be HNO_2 and/or NO. As a matter of fact, the equilibrium $HNO_2 + H_2O \leftrightarrows H_3O^+ + NO_2^-$ (pK_a = 3.3 at 18°C) takes

place. Also, even if HNO_2 disproportionates in a fairly acidic solution, with $3HNO_2 \rightarrow H_3O^+ + NO_3^- + 2NO$, the rate of this reaction is known to be low. **$P_2W_{15}CuAle$** at pH 1 presents the larger cathodic current enhancement (Figure 8) in a potential domain of first wave (Cu^{II}/Cu^{I} couple) compared to **SiW_9CuAle**, **SbW_9CuAle** and **$P_2W_{15}Cu_4$**. The corresponding calculated $J_{kinetic\ (HNO_2)}$ for γ = 10 and 30 at -0.07 V were -49.9 and -103.2 $\mu A.cm^{-2}$ respectively (see SI, Table SI1).

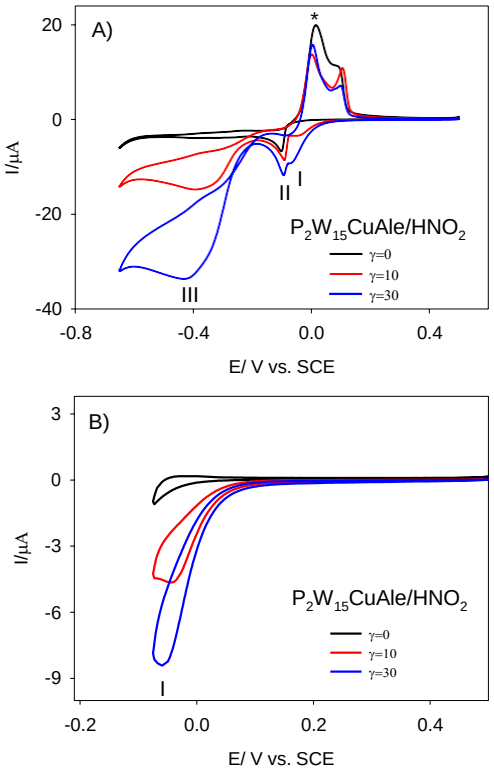

Figure 8. A) Electrocatalysis of NO_2^- reduction in the presence of 0.1 mM **$P_2W_{15}CuAle$** in a pH 1 medium, v = 2 $mV.s^{-1}$, the working electrode was glassy carbon and the reference electrode was SCE. B) Electrocatalysis of NO_2^- reduction with reversal potential fixed after the Cu^{II}/Cu^{I} redox process. * Reoxydation peak of the deposited Cu^0 on electrode surface.

In summary, the four complexes have shown a good efficiency upon the reduction of nitrite, the efficiency being better at pH 1. A significant electrocatalytic activity could be measured already in a potential domain related to the first wave (Cu^{II}/Cu^{I} couple), suggesting that Cu^{I} was already able to reduce HNO_2/NO_2^-.

Conclusion

We have thus reported here the first materials associating polyoxotungstates, bisphosphonates and copper ions. They consist in 1D compounds made of two adjacent anionic $[Cu_6(Ale)_4(H_2O)_4]^{4-}$ and POM units, with a $[Cu_6(Ale)_4(H_2O)_4]^{4-}$/POM ratio depending on the nature of the POM. In **SiW_9CuAle**, an alendronate ligand is directly connected to the $\{Cu_3\}$ fragment capping the POM unit. In contrast, no alendronate is grafted on the POM fragment in **SbW_9CuAle** and **$P_2W_{15}W_9CuAle$**, these compounds being made of pure inorganic POMs connected to $[Cu_6(Ale)_4(H_2O)_4]^{4-}$ clusters. Combining the magnetic studies of **SiW_9CuAle** and **SbW_9CuAle**, it has been possible to evidence the coexistence of ferromagnetic and antiferromagnetic interactions in the $[Cu_6(Ale)_4(H_2O)_4]^{4-}$ unit, while strong antiferromagnetic interactions have been found in the $[SiW_9O_{34}Cu_3(Ale)(H_2O)]^{8-}$ fragment constituting **SiW_9CuAle**. The ability of the three reported compounds to electrocatalytically reduce nitrite and nitrate has been studied. All the studied compounds present a good efficiency upon the reduction of HNO_2 or NO_2^-. In contrast, it has been found that the purely inorganic complex **$Sb_2W_{18}Cu_3$** is inactive toward the reduction of nitrate, highlighting that the formation of a Cu^0 film at the electrode is not sufficient for electrocatalytically reducing NO_3^-. The **SbW_9CuAle** complex is also inactive toward nitrate reduction. As this compound is made of a $\{(SbW_9)_2Cu_3\}$ fragment, similar to that found in **$Sb_2W_{18}Cu_3$**, and $[Cu_6(Ale)_4(H_2O)_4]^{4-}$ units, this evidences that the copper/alendronate cluster is also inactive. In contrast, **SiW_9CuAle** and **$P_2W_{15}CuAle$** have shown a good efficiency as pre-catalysts upon the reduction of NO_3^- either at pH 1 and pH 5, showing that the chemical nature of the POM is a crucial parameter for the catalytic reduction of nitrate by POM species. Interestingly, comparison of the activities of **$P_2W_{15}CuAle$** and $[(P_2W_{15}O_{56})_2Cu_4(H_2O)_2]^{16-}$ evidenced that if the $\{Cu_6(Ale)_4(H_2O)_4\}$ cluster do not act as electrocatalysts, it act as a co-factor, significantly enhancing the catalytic efficiency of the

active POM. Moreover, it must be possible to introduce functional organic or inorganic fragments into the **SiW$_9$CuAle** POM by pre-functionalization of the bisphosphonate via its amino group, as previously shown for cobalt[38] and nickel[14] derivatives. In particular, the grafting of an anchoring organic group onto the bisphosphonate ligand constituting **SiW$_9$CuAle**, allowing to prepare covalently functionalized electrodes, is under study.

ASOCIATED CONTENT

Supporting Information (SI) available: CVs of **P$_2$W$_{15}$CuAle**, **Sb$_2$W$_{18}$Cu$_3$**, **SbW$_9$CuAle** and **SiW$_9$CuAle** in a pH 5 and pH 1 medium. Table of the value of the catalytic efficiency CAT at different values of the excess parameter γ ($\gamma = C^0_{NO_3-}/C^0_{POM}$ or $\gamma = C^0_{HNO_3-}/C^0_{POM}$) in a pH 5 and pH 1 medium. This material is available free of charge via the Internet at http://pub.acs/org.

ACKNOWLEDGMENT

This work was supported by the Ministère de l'Enseignement Supérieur et de la Recherche, the CNRS, the Université de Versailles Saint Quentin en Yvelines, the Université de Strasbourg, the Université Paris XI and a public grant overseen by the French National Research Agency (ANR) as part of the "Investissements d'Avenir" program n°ANR-11-IDEX-0003-02 and the Labex CHARMMMAT ANR-11-LABX-0039. We also thank the Labex CSC of the University of Strasbourg for financial support.

REFERENCES

(1) (a) Miras, H. N.; Yan, J.; Long, D.-L.; Cronin, L. *Chem. Soc. Rev.* **2012**, *41*, 7403. (b) Banerjee, A.; Bassil, B. S.; Röschenthaler, G.-V.; Kortz, U. *Chem. Soc. Rev.* **2012**, *41*, 7590.

(c) Sartorel, A.; Bonchio, M.; Campagna, S.; Scandola, F. *Chem. Soc. Rev.* **2013**, *42*, 2262. (d) Lu, H.; Geletii, Y. V.; Zhao, C.; Vickers, J. W.; Zhu, G.; Luo, Z.; Song, J.; Lian, T.; Musaev, D. G.; Hill, C. L. *Chem. Soc. Rev.* **2012**, *41*, 7572. (e) Proust, A.; Matt, B.; Villanneau, R.; Guillemot, G.; Gouzerh, P.; Izzet, G. *Chem. Soc. Rev.* **2012**, *41*, 7605. (f) Reinoso, S. *Dalton Trans.* **2011**, 6610. (g) Du, D. Y.; Yan, L. K.; Su, Z.-M.; Li, S. L.; Lan, Y. Q.; Wang, E.-B. *Coord. Chem. Rev.* **2013**, *257*, 702.

(2) *Inorganic Syntheses*; Ginsberg, A. P. Ed.; John Wiley and Sons: New York 1990; Vol. 27.

(3) (a) Zheng, S.-T.; Yang, G.-Y. *Chem. Soc. Rev.* **2012**, *41*, 7623. (b) Oms, O.; Dolbecq, A.; Mialane, P. *Chem. Soc. Rev.* **2012**, *41*, 7497.

(4) (a) *Trends in Polyoxometalate Researchs*; Ruhlmann, L. Ed.; Nova Science Publishers: New York 2015. (b) Godin, B.; Chen, Y.-G.; Vaissermann, J.; Ruhlmann, L.; Verdaguer, M.; Gouzerh, P. *Angew. Chem. Int. Ed*. **2005**, *44*, 3072. (c) Al-Oweini, R.; Bassil, B. S.; Friedl, J.; Kottisch, V.; Ibrahim, M.; Asano, M.; Keita, B.; Novitchi, G.; Lan, Y.; Powell, A.; Stimming, U.; Kortz, U. *Inorg. Chem*. **2014**, *53*, 5663. (d) Fang, X.; Speldrich, M.; Schilder, H.; Cao, R.; O'Halloran, K. P.; Hill, C. L.; Kögerler, P. *Chem. Commun*. **2010**, 2760. (e) Zheng, S.-T.; Zhang, J.; Li, X.-X. ; Fang, W.-H. ; Yang, G.-Y. *J. Am. Chem. Soc*. **2010**, *132*, 15102. (f) Rousseau, G.; Oms, O.; Dolbecq, A.; Marrot, J.; Mialane, P. *Inorg. Chem*. **2011**, *50*, 7376.

(5) (a) Wang, J.; Du, J.; Niu, J. *CrystEngComm* **2008**, *10*, 972. (b) Wang, J.; Ma, P.; Shen, Y.; Niu, J. *Cryst. Growth Des.* **2008**, *8*, 3130. (c) Zheng, S.-T.; Yuan, D.-Q.; Jia, H.-P.; Zhang J.; Yang, G.-Y. *Chem. Commun.* **2007**, 1858. (d) Li, B.; Zhao, J.-W.; Zheng S.-T.; Yang, G.-Y. *Inorg. Chem.* **2009**, *48*, 8294. (e) Mialane, P.; Dolbecq, A.; Marrot, J.; Rivière E.; Sécheresse, F. *Chem. Eur. J.* **2005**, *11*, 1771. (f) Artetxe, B.; Reinoso, S.; San Felices, L.; Lezama, L.; Pache, A.; Vicent, C.; Gutiérrez-Zorrilla, J. M. *Inorg. Chem*. **2015**, *54*, 409.

(6) (a) Clemente-Juan, J. M.; Coronado, E.; Gaita-Ariño, A. *Chem. Soc. Rev.* **2012**, *41*, 7464. (b) Kögerler, P.; Tsukerblat, B.; Müller, A. *Dalton Trans*. **2010**, 21.

(7) (a) Ritchie, C.; Ferguson, A.; Nojiri, H.; Miras, H. N.; Song, Y.-F.; Long, D.-L.; Burkholder, E.; Murrie, M.; Kögerler, P.; Brechin, E. K.; Cronin, L. *Angew. Chem., Int. Ed.* **2008**, *47*, 5609. (b) Compain, J.-D.; Mialane, P.; Dolbecq, A.; Mbomekalle, I. M.; Marrot, J.; Sécheresse, F.; Rivière, E.; Rogez G.; Wernsdorfer, W. *Angew. Chem., Int. Ed.* **2009**, *48*, 3077. (c) Ibrahim, M.; Lan, Y.; Bassil, B. S.; Xiang, Y.; Suchopar, A.; Powell, A. K.; Kortz, U. *Angew. Chem., Int. Ed.* **2011**, *50*, 4708. (d) Sawada, Y.; Kosaka, W.; Hayashi Y.; Miyasaka, H. *Inorg. Chem.* **2012**, *51*, 4824. (e) Fang, X.; Kögerler, P.; Speldrich, M.; Schilder H.; Luban, M. *Chem. Commun.* **2012**, 1218. (f) Vonci M.; Boskovic, C. *Aust. J. Chem.* **2014**, *67*, 1542. (g) R. Sato, K. Suzuki, T. Minato, M. Shinoe, K. Yamaguchi, N. Mizuno, *Chem. Commun.* **2015**, *51*, 4081.

(8) (a) Special issue on polyoxometalates with catalytic and electrocatalytic properties: Hill, C. L. Ed., *J. Mol. Catal. A.* **2007**, *262*, 1. See also some recent examples (b) Han, X.-B.; Li, Y.-G.; Zhang, Z.-M.; Tan, H.-Q.; Lu, Y.; Wang, E.-B. *J. Am. Chem. Soc*. **2015,** *137*, 5486. (c) Hao, H.-F.; Zhou, W.-Z.; Zang, H.-Y.; Tan, H.-Q.; Qi, Y.-F.; Wang, Y.-H.; Li, Y.-G. *Chem. Asian J.* **2015**, *10*, 1676. (d) Huo, Y.; Huo, Z.; Ma, P.; Wang, J.; Niu, J. *Inorg. Chem.* **2015**, *54*, 406. (e) Von Allmen, K.; Moré, R.; Müllern R.; Sorinao-López, J.; Linden, A.; Patzke, G. R. *ChemPlusChem* **2015**, *80*, 1389.

(9) Yin, Q.; Tan, J. M.; Besson, C.; Geletii, Y. V.; Musaev, D. G.; Kuznetsov, A. E.; Luo, Z.; Hardcastle, K. I.; Hill, C. L. *Science* **2010**, *328*, 342.

(10) (a) Amanchi, S. R.; Khenkin, A. M.; Diskin-Postner, Y.; Neumann, R. *ACS Catal.* **2015**, *5*, 3336. (b) Anderson, T. M.; Zhang, X.; Hardcastle K. I.; Hill, C. L. *Inorg. Chem.* **2002**, *41*, 2477.

(11) See for example (a) Wang, X.-L.; Li, T.-J.; Tian, A.-X.; Li, N.; Yang, Y.; Ning, Y.-L.; Hou, X. *CrystEngComm.* **2015**, *17*, 3257. (b)Yao, S.; Zhang, Z., Li, Y.; Wang, E. *Dalton Trans.* **2010**, 3884. (c) Mitchell, S. G.; Khanra, S.; Miras, H. N.; Boyd, T.; Long, D.-L.; Cronin, L. *Chem. Commun.* **2009**, 2712. (d) Li, Y.-W.; Li, Y.-G.; Wang, Y.-H.; Feng, X.-J.; Lu, Y.; Wang,

E.-B. *Inorg. Chem.* **2009**, *48*, 6452. (e) Boyd, T.; Mitchell, S. G.; Miras, H. N.; Long, D.-L.; Cronin, L. *Dalton Trans.* **2010**, 6460. (f) Mbomekalle, I. M.; Mialane, P.; Dolbecq, A.; Marrot, J.; Sécheresse, F.; Berthet, P.; Keita, B.; Nadjo, L. *Eur. J. Inorg. Chem.* **2009**, 5194. (g) Ruhlmann, L.; Canny, J.; Contant, R.; Thouvenot, R. *Inorg. Chem.* **2002**, *41*, 3811. (h) Yao, S.; Zhang, Z.; Li, Y.; Wang, E. *Dalton Trans.* **2010**, 3884. (i) Zhang, Z.; Yao, S.; Qi, Y.; Li, Y.; Wang, Y.; Wang, E. *Dalton Trans.* **2008**, 3051.

(12) (a) Zhang, Z.; Qi, Y.; Qin, C.; Li, Y.; Wang, E.; Wang, X.; Su, Z.; Xu, L. *Inorg. Chem.* **2007**, *46*, 8162. (b) Mal, S. S.; Bassil, B. S.; Ibrahim, M.; Nellutla, S.; van Tol, J.; Dalal, N. S.; Fernández, J. A.; López, X.; Poblet, J. M.; Biboum, R. N.; Keita, B.; Kortz, U. *Inorg. Chem.* **2009**, *48*, 11636. (c) Nellutla, S.; van Tol, J.; Dalal, N. S.; Bi, L.-H.; Kortz, U.; Keita, B.; Nadjo, L.; Khitrov, G. A.; Marshall, A. G. *Inorg. Chem.* **2005**, *44*, 9795.

(13) (a) Mal, S. S.; Dickman, M. H.; Kortz, U.; Todea, A. M.; Merca, A.; Bögge, H.; Glaser, T.; Müller, A.; Nellutla, S.; Kaur, N.; van Tol, J.; Dalal, N. S.; Keita, B.; Nadjo, L. *Chem. Eur. J.* **2008**, *14*, 1186. (b) Bi, L.-H.; Kortz, U.; Nellutla, S.; Stowe, A. C.; van Tol, J.; Dalal, N. S.; Keita B.; Nadjo, L. *Inorg. Chem.* **2005**, *44*, 896.

(14) El Moll, H.; Rousseau, G.; Dolbecq, B.; Oms, O.; Marrot, J.; Haouas, M.; Taulelle, F.; Rivière, E.; Wernsdorfer, W.; Lachkar, D.; Lacôte, E.; Keita, B.; Mialane, P. *Chem. Eur. J.* **2013**, *19*, 6753.

(15) Kubíček, V.; Kotek, J.; Hermann P.; Lukeš, I. *Eur. J. Inorg. Chem.* **2007**, 333.

(16) Mialane, P.; Marrot, J.; Rivière, E.; Nebout, J.; Hervé, G. *Inorg. Chem.* **2001**, *40*, 44.

(17) Bösing, M.; Loose, I.; Pohlmann H.; Krebs, B. *Chem. Eur. J.* **1997**, *3*, 1232.

(18) Sheldrick, G. M. SADABS, program for scaling and correction of area detector data, University of Göttingen, Germany, 1997.

(19) Blessing, R. *Acta Crystallogr.***1995**, *A51*, 33.

(20) Sheldrick, G. M. SHELX-TL version 5.03, Software Package for the Crystal Structure Determination, Siemens Analytical X-ray Instrument Division, Madison, WI USA, 1994.

(21) Borras-Almenar, J. J.; Clemente-Juan, J. M.; Coronado, E.; Tsukerblat, B. S. *J. Comput. Chem.* **2001**, *22*, 985.

(22) Woo, H. Y.; So, H.; Pope, M. T. *J. Am. Chem. Soc.* **1996**, *118*, 621.

(23) Bi, L. H.; Kortz, U. *Inorg. Chem.* **2004**, *43*, 7961.

(24) (a) Zheng, S.T.; Yuan, D. Q.; Zhang, J.; Tang, G. Y. *Inorg. Chem.* **2007**, *46*, 4569. (b) Pichon, C.; Mialane, P.; Dolbecq, A.; Marrot, J.; Rivière, E.; Keita, B.; Nadjo, L.; Sécheresse, F. *Inorg. Chem.* **2007**, *46*, 5292.

(25) Li, X. X.; Zheng, S. T.; Fang, W. H.; Yang, G.-Y. *Inorg. Chem. Commun.* **2011**, 1541.

(26) Mialane, P. ; Dolbecq, A.; Marrot, J.; Rivière, E.; Sécheresse, F. *Angew. Chem. Int. Ed.* **2003**, *42*, 3523.

(27) Demoro, B.; Caruso, F.; Rossi, M.; Benítez, D.; González, M.; Cerecetto, H.; Galizzi, M.; Malayil, L.; Docampo, R.; Faccio, R.; Mombrú, Á. W. ; Gambino, D.; Otero, L. *Dalton Trans.* **2012**, 6468.

(28) Weakley, T. J. R.; Finke, R. G. *Inorg. Chem.* **1990**, *29*, 1235.

(29) $R = [\Sigma(\chi MTcalc - \chi MTobs)2/\Sigma(\chi MTobs)2]$

(30) (a) Siedel, A. R.; Padula, F.; Baranowski; Goldstein, C.; DeAngelo, M.; Kokoszka, G. F.; Azevedo, L.; Venturini, E. L. *J. Am. Chem. Soc.* **1983**, *105*, 7447. (b) Stowe, A. C.; Nellutla, S.; Dalal, N. S.; Kortz, U. *Eur. J. Inorg. Chem.* **2004**, 3792.

(31) Crawford, V. H.; Richardson, H. W.; Wasson, J. R.; Hodgson, D. J.; Hatfield, W. E. *Inorg. Chem.* **1976**, *15*, 2107.

(32) Ruiz, E.; Alemany, P.; Alvarez, S.; Cano, J. *J. Am. Chem. Soc.* **1997**, *119*, 1297.

(33) Thompson, L. K.; Mandal, S. K.; Tandon, S. S.; Bridson, J. N.; Park, M. K. *Inorg. Chem.* **1996**, *35*, 117.

(34) Kahn, O. *Inorg. Chim. Acta* **1982**, *62*, 3.

(35) Escuer, A.; Salah El Fallah, M.; Vicente, R.; Sanz, N.; Font-Bardia, M.; Solans, X.; Mautner, F. A. *Dalton Trans.* **2004**, 1867.

(36) (a) Keita, B.; Mbomekalle, I.-M.; Nadjo, L.; Contant, R. *Electrochem. Comm*. **2001**, *3*, 267. (b) Keita, B. ; Abdeljalil, E.; Nadjo, L.; Contant, R.; Belgiche, R. *Electrochem. Comm.* **2001**, *3*, 56. (c) Mbomekalle, I.-M.; Keita, B.; Lu, Y. W. ; Nadjo, L.; Contant, R.; Belai, N.; Pope, M. T. *Eur. J. Inorg. Chem*. **2004**, 4132. (d) Jabbour, D.; Keita, B.; Nadjo, L.; Kortz, U.; Sankar Mal, S. *Electrochem. Comm.* **2005**, *7*, 841. (e) Nellulta, S.; van Tol, J.; Dalal, N. S.; Bi, L.-H.; Kortz, U.; Keita B.; Nadjo, L.; Khitrov, G. A.; Marshall, A. G. *Inorg.Chem*. **2005**, *44*, 9795.

(37) Ruhlmann, L.; Nadjo, L.; Canny, J.; Contant, R.; Thouvenot, R. *Eur. J. Inorg. Chem.* **2002**, 975.

(38) Rousseau, G.; Zhang, S.; Oms, O.; Dolbecq, A.; Marrot, J.; Liu, R.; Shang, X.; Zhang, G.; Keita, B.; Mialane, P. *Chem. Eur. J.*, **2015**, *21*, 12153.

Table 1. Crystallographic data for **SiW_9CuAle**, **SbW_9CuAle** and **$P_2W_{15}CuAle$**.

	SiW_9CuAle	**SbW_9CuAle**	**$P_2W_{15}CuAle$**
Empirical formula	$SiW_9O_{120}Cu_9C_{20}H_{147}N_5P_{10}Na_{12}$	$Sb_4W_{36}Cu_{24}P_{24}C_{48}N_{12}H_{468}ClNa_8Li_{29}O_{396}$	$P_{12}W_{30}Cu_{10}C_{16}H_{148}N_4O_{196}Na_{20}$
Formula weight, *g*	5218.4	17346.2	10515.4
Crystal system	monoclinic	triclinic	monoclinic
Space group	$P2_1/c$	P-1	$P2_1/c$
a / Å	23.3560(8)	22.384(3)	32.256(3)
b / Å	22.4995(8)	32.340(4)	28.454(3)
c /Å	28.2725(9)	34.221(4)	27.131(2)
α / °	90	75.951(4)	90
β / °	99.6330(17)	78.016(5)	93.400(4)
γ / °	90	78.695(5)	90
V / Å^3	14647.7(9)	23229(5)	24857(9)
Z	4	2	4
T / K	200	200	200
ρ_{calc} / g cm^{-3}	2.370	2.304	2.654
μ / mm^{-1}	8.577	10.359	14.838
Data / Parameters	42833 / 1636	82318 / 4165	43911 / 2165
R_{int}	0.0984	0.0954	0.1015
GOF	1.072	1.031	1.037
R (>2σ(I))	R_1[a] = 0.0827	R_1[a] = 0.0918	R_1[a] = 0.0806
	wR_2[b] = 0.1890	wR_2[b] = 0.2469	wR_2[b] = 0.2163

$$^{a}R_1 = \frac{\sum \left||F_o| - |F_c|\right|}{\sum |F_c|} \qquad ^{b}wR_2 = \sqrt{\frac{\sum w(F_o^2 - F_c^2)^2}{\sum w(F_o^2)^2}}$$

Table 2. Reduction and reoxidation peak potentials measured from cyclic voltammograms of **$Sb_2W_{18}Cu_3$**, **SiW_9CuAle**, **SbW_9CuAle** and **$P_2W_{15}CuAle$**.

	Compounds	*	I	II	III	IV
		Cu 0/II	**Cu II/I**	**Cu I/0**	**W VI/V**	
		Ep_a	$E_{1/2}$	Ep_c	$E_{1/2}$	$E_{1/2}$
pH 5	$Sb_2W_{18}Cu_3$	-0.02	-0.13	-0.22	-0.59	-0.81
	SbW_9CuAle	0.03	-0.11	-0.16		
	SiW_9CuAle	0.02	-0.11	-0.16		
	$P_2W_{15}CuAle$	-0.02	-0.14	-0.18	-0.57	
	$P_2W_{15}Cu_4$	-0.02	-0.22	-0.34	-0.58	-0.80
pH 1	$Sb_2W_{18}Cu_3$	0.03	-0.06	-0.12	-0.44	
	SbW_9CuAle	0.05	-0.03	-0.09		
	SiW_9CuAle	0.00	-0.03	-0.11	-0.52	
	$P_2W_{15}CuAle$	0.01	-0.06	-0.10		
	$P_2W_{15}Cu_4$	0.01	-0.10	-0.12	-0.23	-0.31

Potentials in V *vs.* SCE were obtained from cyclic voltammetry in pH 5 medium (1 M $CH_3COOLi+CH_3COOH$) or in pH 1 medium (0.5 M Na_2SO_4 + H_2SO_4 at pH 1). Scan rate = 2 mV s^{-1}. Working electrode: glassy carbon.

Graphic for the Table of Content

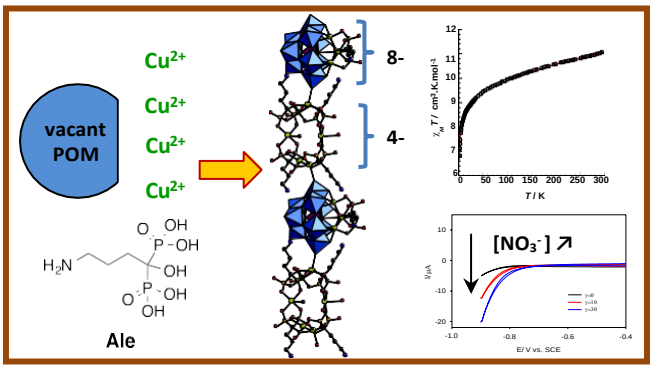

Three 1D compounds where purely inorganic or hybrid copper-substituted polyoxometalates alternate with anionic copper-alendronate complexes have been characterized. Despite the presence of different sub-units, the magnetic interactions characterizing these materials have been fully quantified. Furthermore, while all these compounds are efficient electrocatalysts for the reduction of nitrites, only two of them present a good activity as pre-catalysts for the reduction of nitrates, highlighting the crucial role of the nature of the polyoxometalate. The role of the copper-alendronate entity as a co-factor is also evidenced.